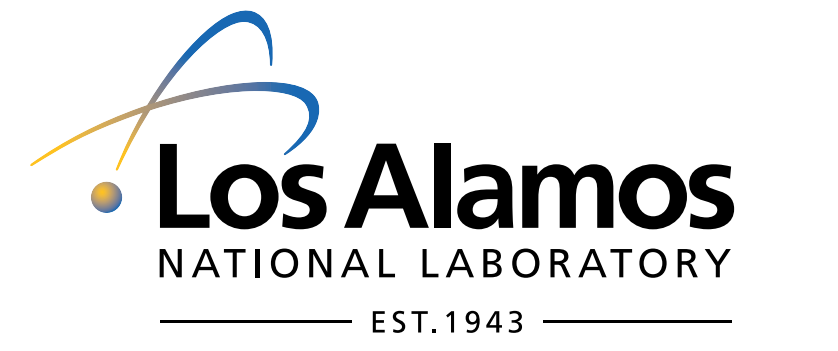


High Resolution Numerical Investigation on the Effect of Convective Instability on Long Term CO₂ Storage in Saline Aquifers

C. Lu and P. Lichtner (PI: lichtner@lanl.gov)



Abstract

CO₂ sequestration (capture, separation, and long term storage) in various geologic media including depleted oil reservoirs, saline aquifers, and oceanic sediments is being considered as a possible solution to reduce greenhouse gas emissions. Dissolution of supercritical CO₂ in formation brines is considered an important storage mechanism to prevent possible leakage. Accurate prediction of the plume dissolution rate and migration is essential. Analytical analysis and numerical experiments have demonstrated that convective instability (Rayleigh instability) has a crucial effect on the dissolution behavior and subsequent mineralization reactions. Global stability analysis indicates that a certain grid resolution is needed to capture the features of density-driven fingering phenomena. For 3-D field scale simulations, high resolution leads to large numbers of grid nodes, unfeasible for a single workstation. In this study, we investigate the effects of convective instability on geologic sequestration of CO₂ by taking advantage of parallel computing using the code PFLORAN, a massively parallel 3-D reservoir simulator for modeling subsurface multiphase, multi-component reactive flow and transport based on continuum scale mass and energy conservation equations. The onset, development and long-term fate of a supercritical CO₂ plume will be resolved with high resolution numerical simulations to investigate the rate of plume dissolution caused by fingering phenomena.

1. Introduction

- Sequestration of CO₂ in subsurface geologic formations containing saline aquifers could provide permanent storage for a major greenhouse gas and thereby help to mitigate global climate change.
- Saline aquifers have an estimated world-wide storage capacity for CO₂ of 320-10,000 Gt CO₂ [1].
- A typical scenario is injection into a relatively deep saline aquifer above the critical point where CO₂ exists as a supercritical fluid ($T_{crit} = 31.104^\circ\text{C}$, $p_{crit} = 73.82$ bar).
- As supercritical CO₂ is injected into the aquifer it becomes buoyant because of its lower density compared to the brine and begins to rise. Eventually it may become trapped by a low permeability zone or caprock and spread laterally as it gradually dissolves into the surrounding brine.
- As the CO₂ dissolves into the brine, the brine becomes heavier and begins to sink resulting in density-driven convection which can lead to instabilities resulting in the formation of CO₂ concentrated brine fingers protruding downward.
- The areal extent of the plume can have an important effect on accidental release of CO₂ to the surface through abandoned bore holes and faults. The areal extent is controlled by competition between the rate of spreading of the plume and the rate at which it dissolves into the brine. Convective mixing can result in much more rapid dissipation of the supercritical CO₂ plume compared to diffusive processes alone.
- It is important to understand the properties of the aquifer which determine the size and onset of fingering during the convective mixing process.
- Analyses of density instability of CO₂ in deep saline aquifers can be used to investigate the onset of convective mixing during CO₂ sequestration in isotropic and anisotropic porous media (Ennis-King and Paterson [4], Xu et al. [8]).
- Linear stability analysis and nonlinear global stability analysis provide complementary approaches: linear stability analysis gives sufficient conditions for the threshold for instability; whereas global stability analysis based on finite perturbations provides a sufficient condition for stability of the CO₂ plume Xu et al. [8].
- Stability analysis can provide rough guidance for determining the conditions of instability and an estimate of the grid size needed to resolve fingering; however, it leaves a number of issues unanswered. For example, a wide gap exists between the prediction of the onset of instability and stability as determined by linear and nonlinear analysis.
- To resolve these issues numerical experiments are performed employing high-resolution grids. The purpose of this work is to provide preliminary results obtained from high-resolution simulations carried out on massively parallel computers and compare these results with the predictions of stability analysis.

2. The Massively Parallel Reactive Flow and Transport Code PFLORAN

- The computer code PFLORAN solves a coupled system of mass and energy conservation equations for a number of phases including H₂O, supercritical CO₂, and black oil, and a gaseous phase. PFLORAN describes coupled thermal-hydrologic-chemical (THC) processes in variably saturated, nonisothermal, porous media in one (1D), two (2D), or three (3D) spatial dimensions.
- The multiphase partial differential equations solved by PFLORAN for mass and energy conservation can be summarized as (Lichtner et al., 1996):

$$\frac{\partial}{\partial t} \left(\phi \sum_{\alpha} s_{\alpha} \rho_{\alpha} X_i^{\alpha} \right) + \nabla \cdot \sum_{\alpha} \left[\mathbf{q}_{\alpha} \rho_{\alpha} X_i^{\alpha} - \phi s_{\alpha} D_{\alpha} \rho_{\alpha} \nabla X_i^{\alpha} \right] = Q_i^{\alpha}, \quad (1a)$$
 and

$$\frac{\partial}{\partial t} \left(\phi \sum_{\alpha} s_{\alpha} \rho_{\alpha} U_{\alpha} + (1 - \phi) \rho_r c_r T \right) + \nabla \cdot \left[\mathbf{q}_{\alpha} \rho_{\alpha} H_{\alpha} - \kappa \nabla T \right] = Q_e. \quad (1b)$$

In these equations, α designates a phase (e.g. H₂O, supercritical CO₂, g), species are designated by the subscript i (e.g. $w = \text{H}_2\text{O}$, $c = \text{CO}_2$), ϕ denotes porosity of the geologic formation, s_{α} denotes the saturation state of the phase; X_i^{α} denotes the mole fraction of species i ; ρ_{α} , H_{α} , U_{α} refer to the molar density, enthalpy, and internal energy of each fluid phase, respectively; \mathbf{q}_{α} denotes the Darcy flow rate defined by

$$\mathbf{q}_{\alpha} = -\frac{k k_{\alpha}}{\mu_{\alpha}} \nabla (p_{\alpha} - W_{\alpha} \rho_{\alpha} g z), \quad (2)$$

where k refers to the water saturated permeability, k_{α} denotes the relative permeability, μ_{α} denotes the fluid viscosity, W_{α} denotes the formula weight, and g denotes the acceleration of gravity. The source/sink terms Q_i^{α} and Q_e , describe injection and extraction at wells.

The density ρ_{α} of fluid phase α appearing in Eqns. (1a) and (1b) refers to the density of the fluid mixture. Use of ideal mixing for the system H₂O-CO₂ leads to a lower density of the mixture. In this work the correlation developed by Garcia [5] is used which gives a greater mixture density in agreement with experiment [5]. Finally, a Henry's law relation from [3] is used to compute the equilibrium concentration of CO₂ dissolved in H₂O of the form

$$X_i^{\beta} = K_{i,\beta\alpha} X_i^{\alpha}, \quad (3)$$

with Henry constant $K_{i,\beta\alpha}$, with $i = \text{CO}_2$, $\alpha = \text{CO}_2(\text{g})$, and $\beta = \text{H}_2\text{O}$.

- The multicomponent reactive transport equations solved by PTRAN have the form (Lichtner et al., 1996):

$$\frac{\partial}{\partial t} \left(\phi \sum_{\alpha} s_{\alpha} \Psi_j^{\alpha} \right) + \nabla \cdot \sum_{\alpha} \Omega_j^{\alpha} = - \sum_m \nu_{jm} I_m, \quad (4)$$

for the j th primary species, and

$$\frac{\partial \phi_m}{\partial t} = \bar{\nu}_m I_m, \quad (5)$$

for the m th mineral.

- Definitions: Ψ_j^{α} , Ω_j^{α} denote the total concentration and flux, defined by the expressions

$$\Psi_j^{\alpha} = \delta_{\alpha j} C_j^{\alpha} + \sum_i \nu_{ji} C_i^{\alpha}, \quad (6)$$

and

$$\Omega_j^{\alpha} = (-\tau \phi s_{\alpha} D_{\alpha} \nabla + \mathbf{q}_{\alpha}) \Psi_j^{\alpha}, \quad (7)$$

where C_j^{α} denotes the solute concentration in phase α , C_i^{α} denotes the concentration of the i th secondary species related to the concentration of primary species through the mass action equations

$$C_i^{\alpha} = (\gamma_i^{\alpha})^{-1} K_i^{\alpha} \prod_j (\gamma_j^{\alpha} C_j^{\alpha})^{\nu_{ij}}, \quad (8)$$

where γ_i^{α} denotes the activity coefficient, and K_i^{α} denotes the equilibrium constant for the reaction.

- The mineral concentration is represented by the volume fraction ϕ_m with molar volume \bar{V}_m . The kinetic reaction rate I_m for the m th mineral is assumed to have the form

$$I_m = -k_m A_m \Phi(\phi_m) (1 - K_m Q_m), \quad (9)$$

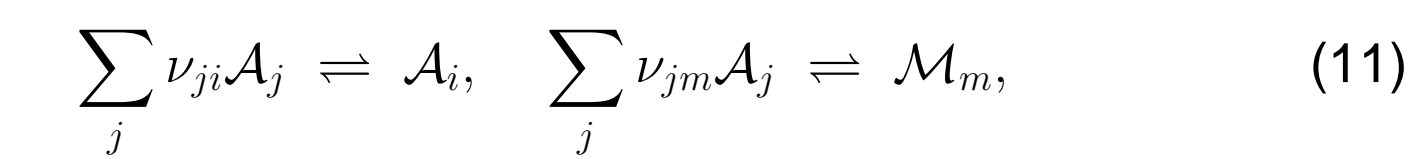
based on transition state theory, where k_m denotes the kinetic rate constant, K_m denotes the equilibrium constant for reaction (11), A_m

the mineral specific surface area, and Q_m the ion activity product defined by

$$Q_m = \prod_j (\gamma_j^{\alpha} C_j^{\alpha})^{\nu_{jm}}. \quad (10)$$

The factor $\Phi(\phi_m)$ is unity if $\phi_m > 0$ or $K_m Q_m > 1$, and zero otherwise, where ϕ_m denotes the mineral volume fraction. The sign of the rate is positive for precipitation and negative for dissolution and vanishes at equilibrium when $K_m Q_m = 1$.

- Chemical reactions included in PTRAN involve homogeneous and heterogeneous reaction between aqueous species and minerals which can be written in the general forms



respectively, where the set of species $\{A_j\}$ refer to a set of primary or basis species in terms of which all other species are written, A_i denotes an aqueous complex referred to as a secondary species, and \mathcal{M}_m refers to a mineral.

- The corresponding thermodynamic equilibrium constants K_i , K_m , and reaction stoichiometric coefficients ν_{ji} , ν_{jm} are derived from an extensive database for aqueous species, gases, and minerals.

- Partitioning CO₂ between H₂O and supercritical CO₂ is accomplished with the reaction



where the subscript (g) refers to the supercritical phase and (aq) to the aqueous phase. Other reactions not include above that may also significantly impact CO₂ sequestration are ion exchange and surface complexation reactions.

3. Parallel Implementation

- PFLORAN is written from the ground up to run on massively parallel computer architectures (Hammond et al., 2005).
- Parallelization is implemented through the PETSc parallel library developed at Argonne National Laboratory (Balay et al., 1997).
- PETSc provides a user friendly set of routines for solving systems of nonlinear equations in parallel using domain decomposition [Figure 1(a)].
- This includes parallel solvers and preconditioners, parallel construction of the Jacobian matrix and residual function, and seamless message passing, which together provide a high parallel efficiency.
- PETSc (latest version 2.3.2) has achieved a high level of maturity that allows rapid development with efficient parallel implementation for solving systems of non-linear partial differential equations.
- PFLORAN makes use of object-oriented features in FORTRAN 90 and is essentially platform independent, running on any machine that PETSc runs on. This includes laptop computers, workstations, and massively parallel high performance computing facilities.

Flow of Control for PDE Solution

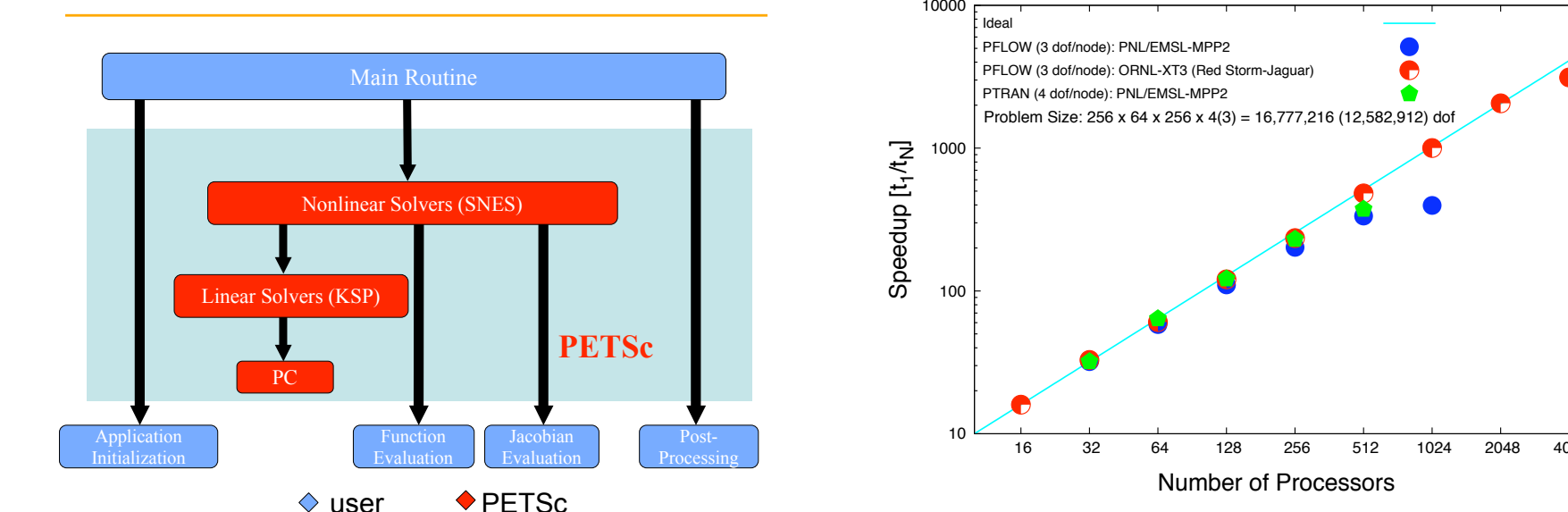


Figure 1: PETSc provides message passing capabilities, solvers and preconditioners for parallel computing (left). The user supplies the residual function and Jacobian. Performance of PFLORAN and PTRAN (right) running a single phase thermo-hydrologic benchmark problem on a 256 × 64 × 256 grid with three and four degrees of freedom per node, respectively (approximately 12.6 and 16.8 million degrees of freedom total).

Sample parallel strong scaling is shown in Figure 1(b) for a modest sized problem running on MPP2 at PNNL/EMSL and Jaguar at ORNL (Mills et al., 2005). The benchmark was run on both the MPP2 cluster at PNNL/EMSL, a cluster of 1960 1.5 GHz Itanium 2 processors with Quadrics QsNetIII interconnect, and Jaguar, the 5294 Opteron processor Cray XT3 at ORNL/NCCS. PFLORAN scales quite well on both machines, bottoming out at around 1024 processors on MPP2, and scaling exceptionally well on Jaguar, displaying linear speedup all the way up to 2048 processors, and still displaying good speedup when going from there to 4096 processors. PTRAN scales similarly, which is not surprising because its computational structure is nearly identical to that of PFLORAN.

4. Convective Mixing

4.1 Stability Analysis

Theoretical linear stability analysis predicts the critical wavelength and time for instability ranging from millimeters to meters and seconds to hundreds of years depending on a number of factors. These include the permeability and porosity of the rock formation k and ϕ , the fluid viscosity μ , effective diffusivity D , the acceleration of gravity g , and the difference in fluid densities $\Delta\rho$ between the CO₂-rich solution and the formation water according to the relation [8]

$$\lambda_c = C_{\lambda} \frac{\mu \phi D}{k g \Delta\rho}, \quad (13)$$

for the critical wavelength λ_c , where C_{λ} is a constant approximately equal to 96.23. The critical time τ_c for the onset of instability is found to be

$$\tau_c = C_{\tau} \left(\frac{\mu \phi}{k g \Delta\rho} \right)^2 D, \quad (14)$$

with $C_{\tau} = 75.19$. The critical wavelength and time are related by

$$\lambda_c = \frac{C_{\lambda}}{\sqrt{C_{\tau}}} \sqrt{D \tau_c}. \quad (15)$$

Noteworthy, is that the critical wavelength is independent of the aquifer thickness. A plot of Eqns.(13) and (14) is shown in Figure 2 as a function of permeability with fixed values for porosity $\phi=0.2$, viscosity $\mu=5 \times 10^{-4}$ Pa·s, effective diffusivity $D=10^{-9}$ m²/s, acceleration of gravity $g=9.8$ m/s², and density difference $\Delta\rho=10$ kg/m³.

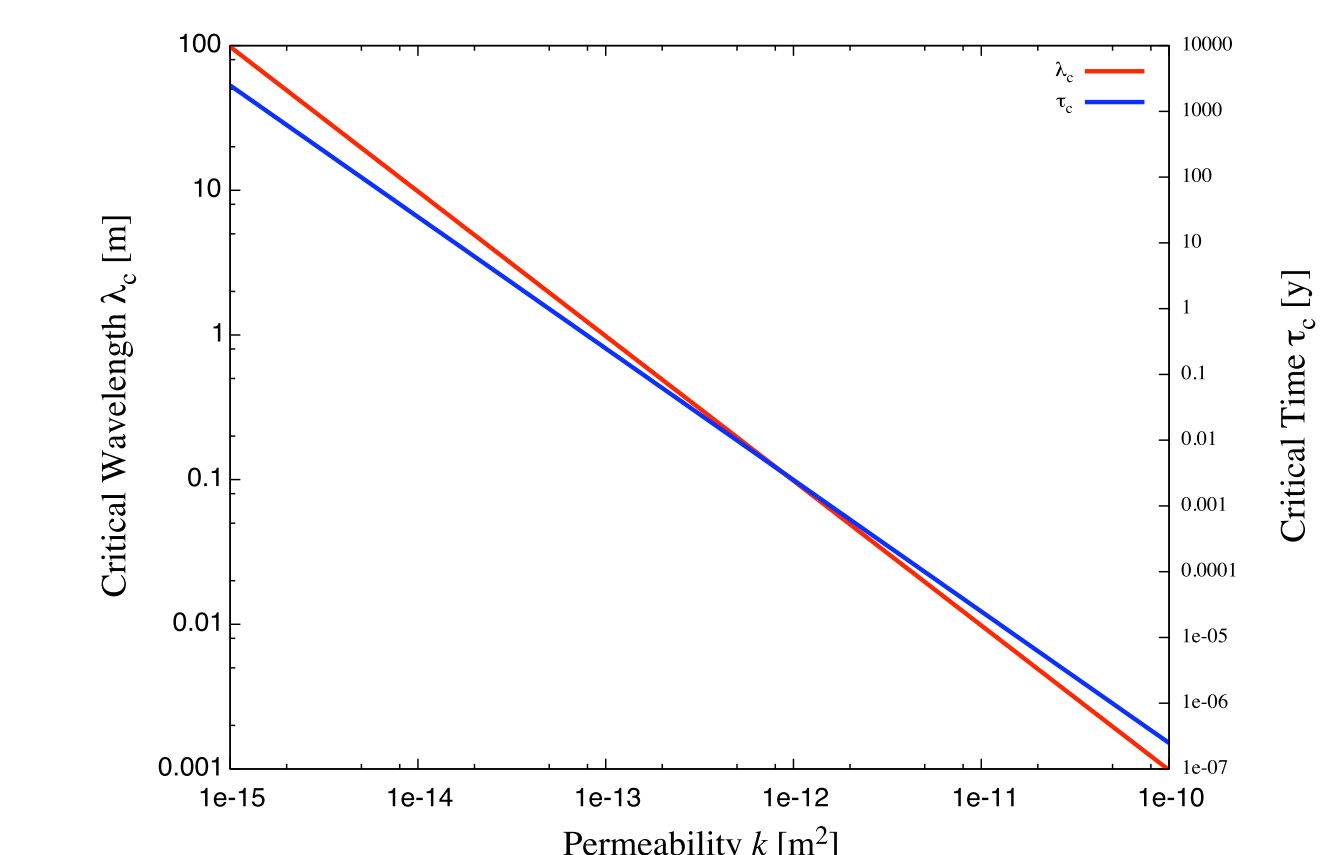


Figure 2: Critical wavelength λ_c and time τ_c as a function of permeability.

4.2 PFLORAN Simulations

Two 3D simulations are presented involving a coarse and fine grid. In both simulations an isotropic permeability of 2×10^{-12} m² is used with a porosity of 15%. The nominal temperature and pressure is 50°C and 200 bars. The computational domain is 250 m thick and 7 × 7 km in lateral extent. CO₂ is injected at a depth of 50 m below the top of the domain. No flow boundary conditions are imposed at the top and bottom and front and back of the domain with constant pressure at the left and right sides. An injection rate of 1 Mt/y for 20 years was used in the simulations. This corresponds to roughly 75% of the CO₂ produced by a 1000 MW gas-fired power plant in 20 years.

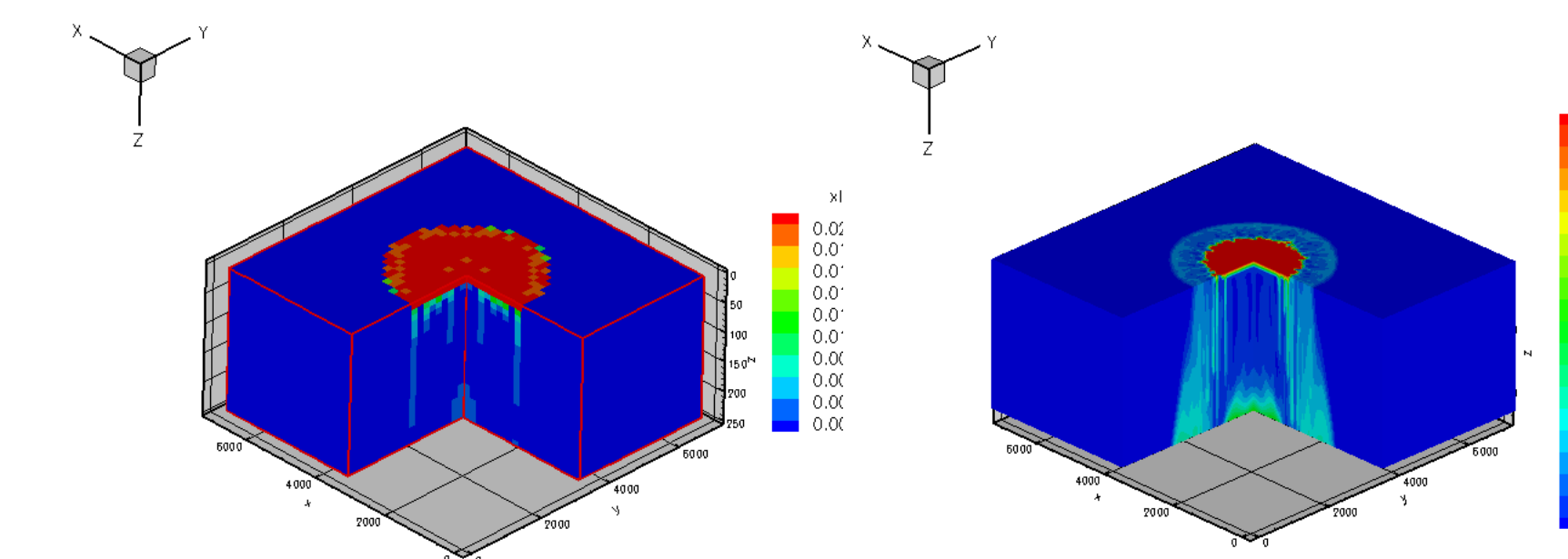


Figure 3: (a) Coarse grid.

Figure 3: (b) Fine grid.

Shown in Figure 3 is the dissolved CO₂ mole fraction corresponding to an elapsed time of 300 years calculated on a coarse-grid with 40×40×25 nodes. The grid spacing is 175 m horizontally and 10 m vertically. In Figure 3 the grid is refined in the x and y directions by a factor 4 with the same grid spacing in the z direction. For both simulations the finger width is equal to the horizontal grid spacing indicating that convergence is not obtained. Indeed, for the parameters used in the simulations, according to stability analysis the critical wavelength should be on the order of $\lambda_c = 0.05$ m and $\tau_c = 6.2 \times 10^{-4}$ y. This is much too small to resolve even with the fastest computers using a uniform grid.

In Figure 4(a) the total mols of CO₂ is plotted as a function of time for both coarse and fine grids showing the amount of CO₂ dissolved in the brine and as supercritical CO₂. The supercritical phase disappears at approximately 400 years for the fine grid compared to 800 years for the coarse grid in the 3D simulations. A slight increase in total CO₂ occurs due to the dissolution of calcite cement resulting from acid produced by injection of supercritical CO₂. In Figure 4(b) the results of 2D simulations are shown for supercritical CO₂ illustrating convergence as the grid is refined.

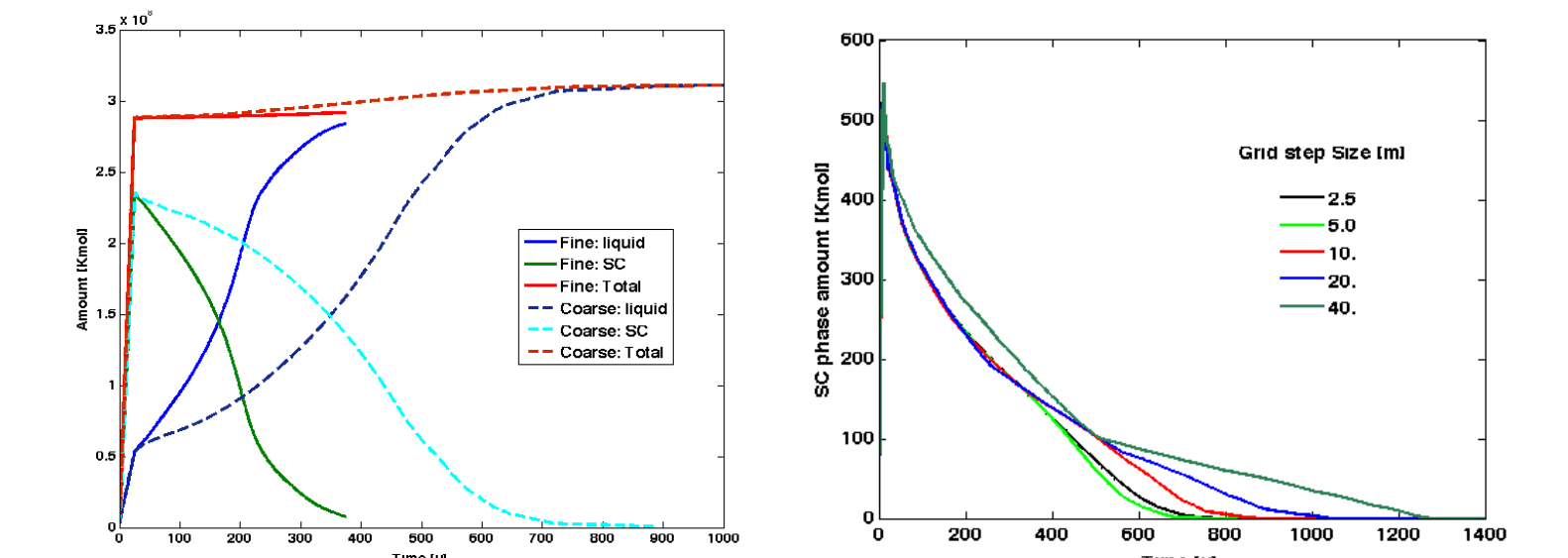


Figure 4: (a) 3D simulation.

Figure 4: (b) 2D simulation.

5. Conclusion

- The calculated rate of dissolution of CO₂ into the formation brine of a saline aquifer in which supercritical CO₂ is injected was found to be highly dependent on grid resolution because of density-driven instabilities resulting in fingering of the dissolved CO₂.
- According to stability analysis, finger width can range over many orders of magnitude and for highly permeable regions may be too small to resolve even with massively parallel computing architectures.
- Numerical experiments utilizing massive parallel computing can provide the basis for formulating such upscaling relations.

Acknowledgments

We would like to thank members of the SciDAC-2 team Glenn Hammond, Richard Mills, David Moulton, Bobby Philip, Barry Smith and Al Valocchi for helpful discussions. R. Mills provided the speedup curve on Jaguar.

References

- [1] Bachu S 2002 Sequestration of CO₂ in geological media in response to climate change: road map for site selection using the transform of the geological space into the CO₂ phase space. *Energy Convers. Manag.* **43** 87–102.
- [2] Balay, S., W.D. Gropp, L.C. McInnes and B.F. Smith (1997) Efficient Management of Parallelism in Object Oriented Numerical Software Libraries, Modern Software Tools in Scientific Computing, Ed. E. Arge, A. M. Bruaset and H. P. Langtangen, 163-202, Birkhauser Press.
- [3] Duan Z and Sun R 2003 An improved model calculating CO₂ solubility in pure water and aqueous NaCl solutions from 273 to 533 K and from 0 to 2000 bar, *Chem. Geol.* **193** 257–271.
- [4] Ennis-King J and Paterson L 2003 Role of convective mixing in the long-term storage of carbon dioxide in deep saline formations. In: SPE annual technical conference and exhibition, SPE 84344, Denver Colorado.
- [5] Garcia J E 2001 Density of aqueous solutions of CO₂, Technical Report LBNL-49023, Lawrence Berkeley National Laboratory, Berkeley, CA.
- [6] Lichtner P C 1996 Continuum Formulation of Multicomponent-Multiphase Reactive Transport, In: *Reactive Transport in Porous Media* (eds. P. C. Lichtner, C. I. Steefel, and E. H. Oelkers), *Reviews in Mineralogy*, **34**, 1–81.
- [7] Mills, R.T., C. Lu, and P.C. Lichtner (2005) PFLORAN: A massively parallel simulator for reactive flows in geologic media, SC2005.
- [8] Xu X, Chen S and Zhang D 2006 Convective stability analysis of the long-term storage of carbon dioxide in deep saline aquifers, *Adv. Wat. Res.* **29** 397–407.